THE ASTROPHYSICAL JOURNAL, 463:L97–L100, 1996 June 1

LYNDS 1527: AN EMBEDDED PROTOBINARY SYSTEM IN TAURUS

G. A. FULLER[1, 2]
National Radio Astronomy Observatory,[3] Edgemont Road, Charlottesville, VA 22903
E. F. LADD
Five College Radio Astronomy Observatory, 619 Lederle Graduate Research Center, University of Massachusetts, Amherst, MA 01003
AND
K.-W. HODAPP
Institute for Astronomy, University of Hawaii, 2680 Woodlawn Drive, Honolulu, HI 96822
Received 1995 December 5; accepted 1996 March 11

ABSTRACT

Submillimeter continuum maps at 800 μm of the embedded source IRAS 04368+2557 in L1527 in Taurus show that there are two sources separated by 20″, or 2800 AU. The secondary source is between 2 and 3 times less luminous than the primary source if both sources have similar spectral energy distributions. Large-scale $C^{18}O$ $J = 1 \rightarrow 0$ emission shows the sources to be embedded in a single dense core, and observations of $C^{18}O$ and $C^{17}O$ show the sources to be associated with a compact region of high-density gas. Three transitions of $C^{18}O$ show a velocity gradient between the two sources. On the smallest size scale, the $C^{18}O$ $J = 3 \rightarrow 2$ emission has a velocity gradient of 3–7 km s^{-1} pc^{-1}. The proximity of the sources in both space and velocity suggest that they are a very young protobinary system. The estimated age of the primary source, 5×10^3 yr, is much less than the estimated orbital period, 1.4×10^5 yr. The separation and young age of the system indicates that it formed through fragmentation of the dense core during collapse.

Subject headings: ISM: individual (L1527) — stars: formation

1. INTRODUCTION

Recent surveys have begun to reveal that companions to T Tauri stars are at least as common, if not more common than, companions to main-sequence stars. These results suggest that all low-mass stars may have companions by the time they reach the T Tauri stage of evolution (Mathieu, Walter, & Myers 1988; Simon et al. 1992, 1995; Reipurth & Zinnecker 1993; Ghez, Neugebauer, & Matthews 1993; Leinert et al. 1993).

Despite the relatively high frequency of binaries in the later phases of star formation, few binary or protobinary systems are known among the most deeply embedded and presumably youngest sources. This apparent difference in the frequency of binaries as a function of system age has led to the suggestion that binaries form relatively late in the star formation process, either by fragmentation of a circumstellar disk (Adams, Ruden, & Shu 1989; Shu et al. 1990) or by disk-aided capture (Clarke & Pringle 1991). However, the detection of multiplicity in very young systems is complicated by the fact that these sources are only detectable in the far-infrared and submillimeter bands, where telescope beam sizes are large and wide field mapping is difficult. Thus, the true binary frequency among the very youngest sources is not well known, and it is entirely possible that binary systems are common even at the earliest stages of star formation.

In this Letter, we report the discovery of a very young embedded protobinary system in the Lynds 1527 dark cloud in Taurus. The properties of this binary system, and in particular its young age, indicate that the binary has formed during, rather than after, the initial collapse of the dense core in which it is forming.

IRAS 04368+2557 is a bright far-infrared and submillimeter wavelength source that is invisible at optical wavelengths and is only seen as a reflection nebula in the near-infrared. Its spectral energy distribution has a bolometric temperature of 59 K (Myers & Ladd 1993), making it the youngest source included in the compilation of Taurus sources by Chen et al. (1995). From modeling of the source spectral energy distribution (SED), Kenyon, Calvet, & Hartmann (1993) derived an age of 4.6×10^3 yr for the source. The age can also be estimated from the dynamical age of the outflow, 20×10^3 yr, based on the outflow's velocity and size (MacLeod et al. 1994). Although Parker, Padman, & Scott (1991) have argued that the dynamical ages of outflows can underestimate the true age of a source by an order of magnitude, this does not appear to be the case for IRAS 04368+2557, since the SED-derived age is significantly smaller than the outflow-derived age. This may be because IRAS 04368+2557 is considerably younger than the outflows Parker et al. (1991) studied.

2. OBSERVATIONS AND DATA REDUCTION

The 800 μm continuum emission from IRAS 04368+2557 has been mapped with the James Clerk Maxwell Telescope (JCMT)[4] in Hawaii, and in various transitions of $C^{18}O$ and $C^{17}O$ with the Five College Radio Astronomy Observatory

[1] Jansky Fellow.
[2] Present address: Department of Physics, UMIST, P.O. Box 88, Manchester, M60 1QD, UK.
[3] The National Radio Astronomy Observatory is a facility of the National Science Foundation operated under cooperative agreement by Associated Universities, Inc.
[4] The James Clerk Maxwell Telescope is operated by The Observatories on behalf of the Particle Physics and Astronomy Research Council of the United Kingdom, the Netherlands Organisation for Scientific Research, and the National Research Council of Canada.

TABLE 1

JOURNAL OF OBSERVATIONS

Telescope	Date	Probe	Frequency (GHz)	Beam Size (arcsec)
JCMT	1995 Sep 28	800 μm	375	13.6
CSO	1995 Sep 6–7	$C^{18}O$ $J = 3 \rightarrow 2$	329.330566	23
JCMT	1995 Sep 26–27	$C^{18}O$ $J = 2 \rightarrow 1$	219.560369	23
		$C^{17}O$ $J = 2 \rightarrow 1$	224.7142	23
FCRAO	1994 Oct–1995 Feb	$C^{18}O$ $J = 1 \rightarrow 0$	109.782182	60
		$C^{17}O$ $J = 1 \rightarrow 0$	112.358981	60

14 m telescope (FCRAO),[5] JCMT, and the Caltech Submillimeter Observatory 10 m telescope (CSO).[6] The details of the observations are given in Table 1.

Except for the $C^{18}O$ $J = 3 \rightarrow 2$ map, the spectral line maps shown in the figures were made with half-beamwidth or better sampling. The data have been convolved down to beam sizes of 26″ for the $J = 2 \rightarrow 1$ transitions and 60″ for the $J = 1 \rightarrow 0$ maps. The 800 μm map was made using on-the-fly mapping. Ten individual maps were made of the source by raster scanning the telescope across the source, while chopping 32″ in azimuth at 7.8 Hz. These maps were sampled on 4″ cells. The FWHM beam size of the observations, as determined from maps of Uranus, is 13.″6. The individual maps were calibrated against measurements of Uranus and the nearby secondary calibrator L1551 IRS 5 (Sandell 1994; Ladd et al. 1995) and averaged together to produce the map shown in Figure 1. While reducing the data, each map was individually inspected, and both the main source and companion were visible in most of the individual maps.

3. RESULTS

The 800 μm emission from IRAS 04368+2557 is resolved into two components, separated by about 20″ (Fig. 1 [Pl. L6]). The brighter peak in the map, L1527A, agrees well in position with the compact 2.7 mm continuum source detected by Terebey, Chandler, & André (1993) and Wilner et al. (1996). A second source, L1527B, with a peak flux about 2.5 times weaker than that of the brighter source, is clearly detected about 20″ northwest (P.A. = −64°) of the brighter source. The positions, sizes, and integrated fluxes of both sources, determined from simultaneous two-dimensional Gaussian fits to the 800 μm map, are given in Table 2.

Adopting a temperature of 26 K as a characteristic temperature for the dust around L1527A (Ladd et al. 1991b), the integrated 800 μm flux indicates the presence of 0.46 $M_\odot$ of material within a radius of 1000 AU, adopting the dust opacity from Pollack et al. (1994). If L1527A and L1527B have similar submillimeter continuum spectra, the ratio of the masses of circumstellar dust around the two sources is given by their integrated flux ratio (2.6:1), giving a circumstellar dust mass for L1527B of 0.18 $M_\odot$.

Both continuum sources are located within one FWHM beamwidth of the peak of the well-defined core detected in the integrated $C^{18}O$ and $C^{17}O$ $J = 1 \rightarrow 0$ intensity (Fig. 2 [Pl. L7]). At higher spatial resolution, and on smaller size scales, the maps of the $C^{18}O$ $J = 2 \rightarrow 1$ and $J = 3 \rightarrow 2$ and $C^{17}O$ $J = 2 \rightarrow 1$ (Fig. 3 [Pl. L8]) show the sources to be even closer to the core peak. All three high-frequency line maps peak closer to L1527A than to L1527B, but the $C^{18}O$ $J = 2 \rightarrow 1$ map is elongated with an axial ratio of about 2:1 in the direction of the second source. In the $C^{17}O$ map, L1527A is located at the peak of a nearly north-south ridge of emission, which has an extension from the northwestern edge that encompasses L1527B. The $C^{18}O$ $J = 3 \rightarrow 2$ emission shows a bright peak close to L1527A and a second peak northwest of L1527B, which sits in a minimum between the two peaks.

All three $C^{18}O$ transitions show evidence of a velocity gradient in the region close to the L1527A/B system. The magnitude and direction of the velocity gradients in the $J = 1 \rightarrow 0$ and $J = 2 \rightarrow 1$ transitions of $C^{18}O$ were determined using the method discussed by Goodman et al. (1993). Gaussian fits to the central region of each line (5.5–6.5 km s^{-1}) were used to determine the line-center velocity. Velocity gradients of 1.60 ± 0.01 km s^{-1} pc^{-1}—at a position angle of 125° ± 1° east of north (the direction of increasing velocity)—and 2.40 ± 0.03 km s^{-1} pc^{-1}—at a position angle of 128° ± 1° east of north—were measured in $J = 1 \rightarrow 0$ line and in the $J = 2 \rightarrow 1$ lines, respectively.[7] In both cases the velocity gradient is nearly parallel to the line joining the two continuum sources.

Position-velocity maps along the binary axis in all three $C^{18}O$ transitions are shown in Figure 4 (Plate L9). Each of the

[5] The Five College Radio Astronomy Observatory is operated with support from the National Science Foundation under grant AST 94-20159 and with the permission of the Metropolitan District Commission of Massachusetts.

[6] Work at the Caltech Submillimeter Observatory is funded by the National Science Foundation under contract AST 93-13929.

[7] The $C^{18}O$ $J = 3 \rightarrow 2$ map has a velocity gradient of 2.22 ± 0.05 km s^{-1} pc^{-1}, at a position angle of 94° ± 1°; however, it is clear from inspection of the individual spectra that this gradient is strongly affected by the outflow from L1527A. The position-velocity map discussed below is less affected by the outflow, which is confined along the east-west direction.

TABLE 2

PROPERTIES OF SOURCES

Source	R.A. (1950)	Decl. (1950)	800 μm Flux: Peak (Jy)	800 μm Flux: Integrated (Jy)	Size (arcsec)	P.A. (E of N)	Mass[a] ($M_\odot$)
L1527A	$04^h36^m49^s.5$	+25°57′22″	1.3	2.6	25 × 15	8°	0.20–0.46
L1527B	04 36 48.2	+25 57 33	0.5	1.3	31 × 15	172	0.08–0.18

[a] Mass from integrated flux using dust opacity $\kappa_\nu = 0.005(1000/\lambda_{\mu m})^{1.5}$ (Pollack et al. 1994) for temperatures from 50 to 26 K.

PLATE L6

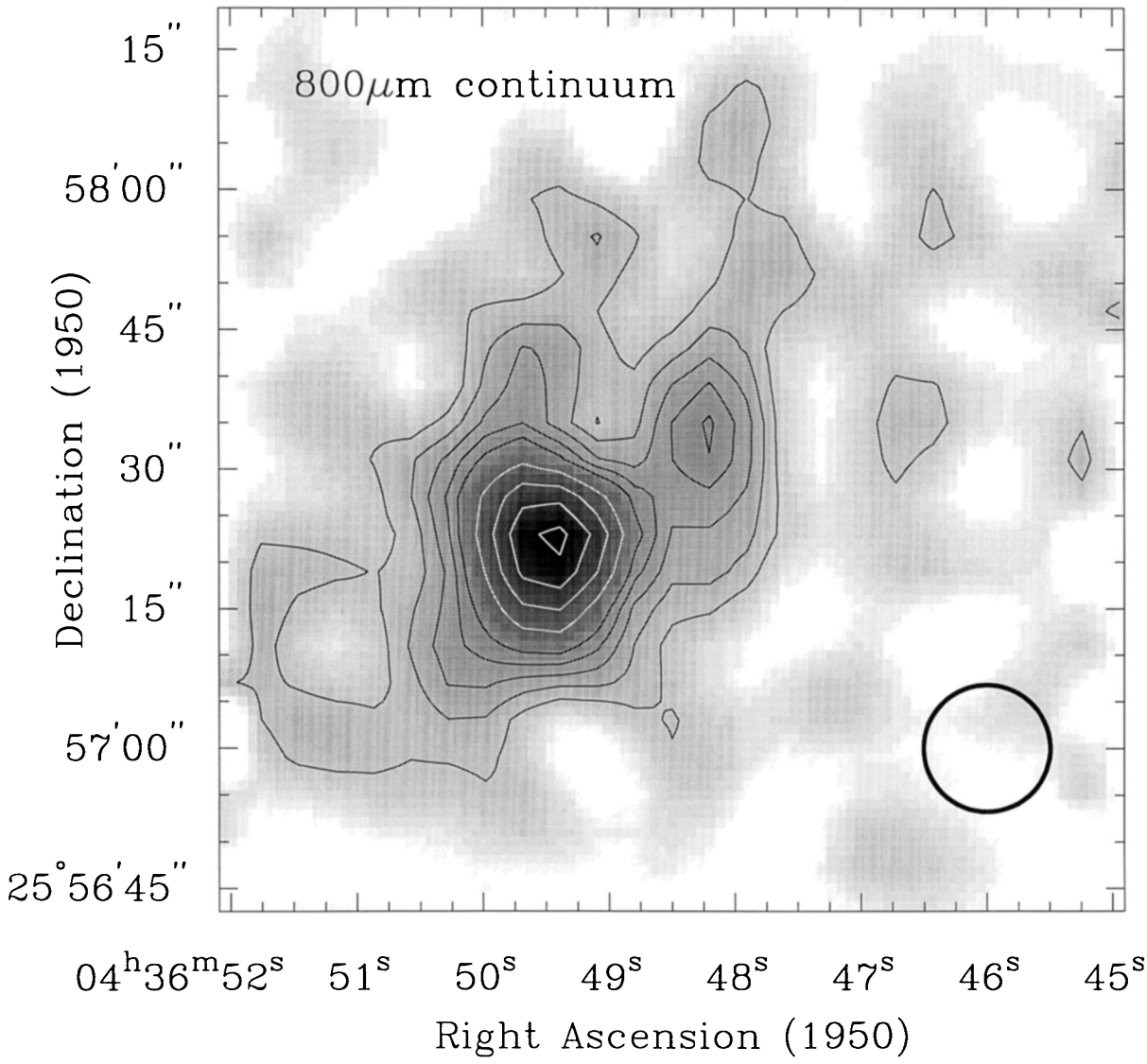

FIG. 1.—Map of the 800 μm continuum emission from IRAS 04368+2557. The position of the brighter source (L1527A) agrees well with the position of the compact source detected by Terebey et al. (1993). The newly detected companion source, L1527B, is evident to the northwest of L1527A. Contours start at 0.2 Jy beam^{-1} and increase in steps of 0.1 Jy beam^{-1}. The rms noise level in the map is 0.07 Jy beam^{-1}. The beam has a FWHM size of 13.″6, and it is shown in the lower right corner.

FULLER, LADD, & HODAPP (see 463, L98)

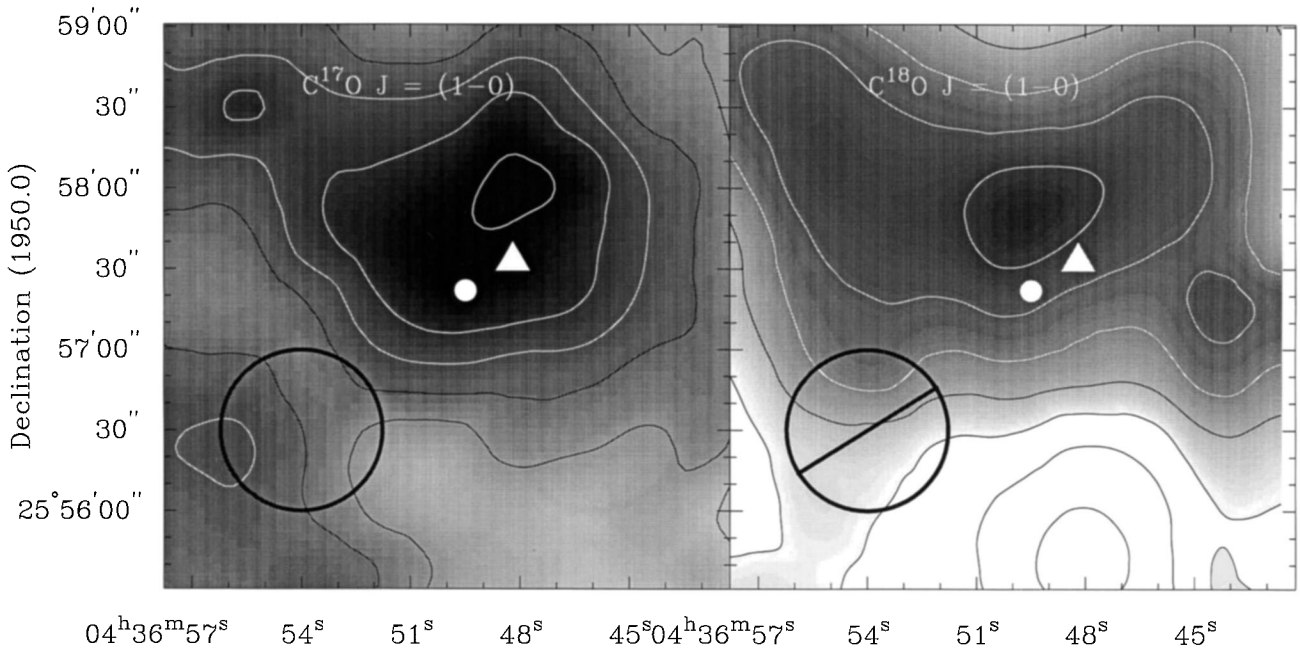

FIG. 2.—Maps of the integrated intensity of $C^{18}O$ (*right*) and $C^{17}O$ (*left*) $J = 1 \rightarrow 0$ emission toward IRAS 04368+2557 from the FCRAO 14 m telescope. Locations of L1527A and L1527B are indicated by the star and triangle, respectively. Data were originally taken with a 48″ beam on a 25″ grid, and have been convolved to 60″ resolution. Beam sizes are indicated by the circles in the lower left of each panel. The line through the circle in the $C^{18}O$ panel indicates the position angle of the velocity gradient found in these data. Contour levels for the $C^{17}O$ map start at 0.2 K km s^{-1} and increment by 0.05 K km s^{-1}. Contour levels for the $C^{18}O$ map start at 0.7 K km s^{-1} and increment by 0.1 K km s^{-1}.

FULLER, LADD, & HODAPP (see 463, L98)

PLATE L8

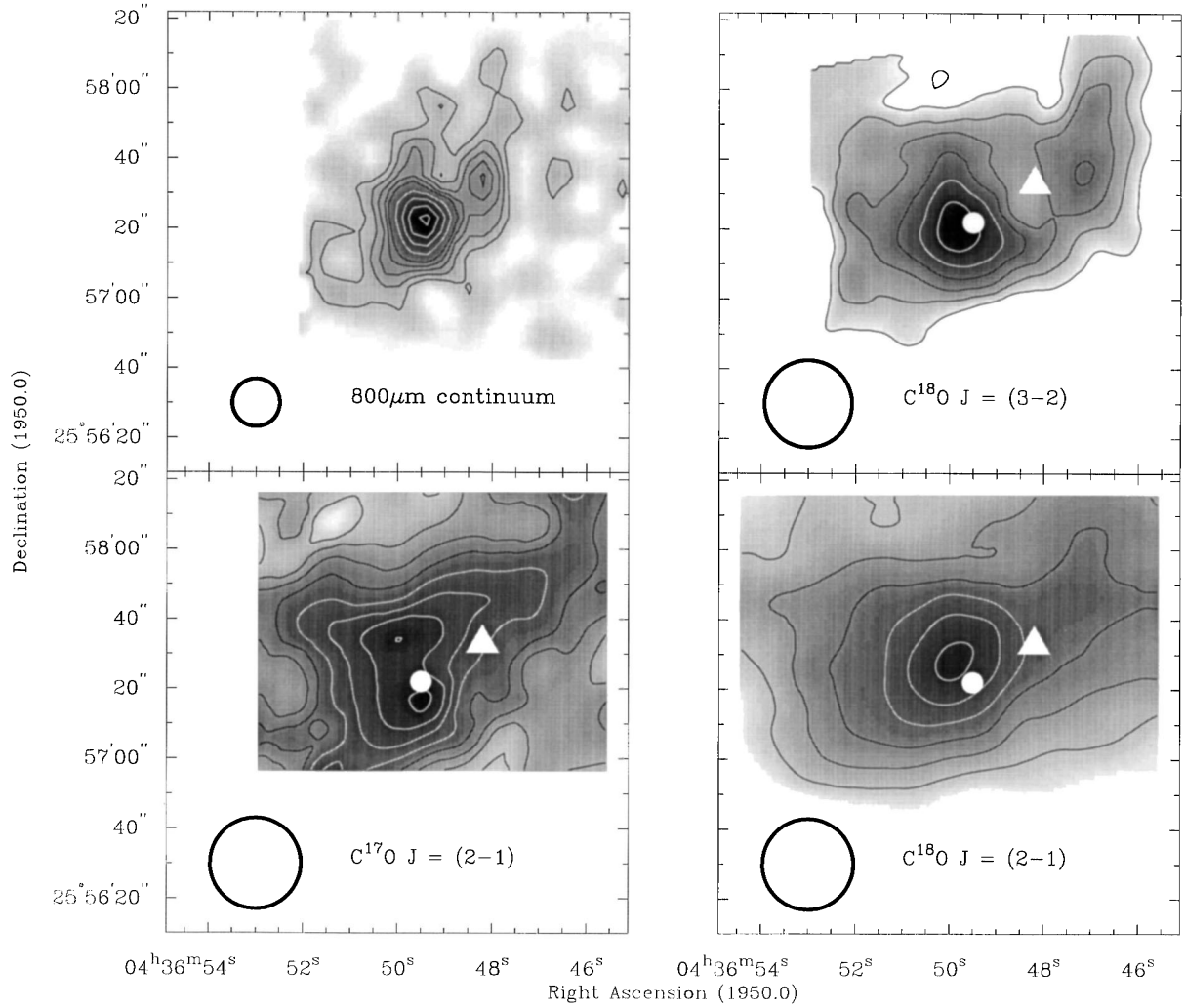

FIG. 3.—Maps of the 800 μm continuum emission (*upper left*), the integrated intensity of the $C^{18}O$ $J = 3 \rightarrow 2$ line (*upper right*), the integrated intensity of the $C^{18}O$ $J = 2 \rightarrow 1$ line (*lower right*), and the integrated intensity of a Gaussian fit to the nine $C^{17}O$ $J = 2 \rightarrow 1$ hyperfine components (*lower left*). The 800 μm contours are as in Fig. 1. The $C^{18}O$ $J = 3 \rightarrow 2$ emission was integrated over the velocity range 5.4–6.4 km s^{-1} to avoid contributions from high-velocity emission associated with the outflow from L1527A. Contours begin at 0.5 K km s^{-1} and increment by 0.1 K km s^{-1}. The same velocity limits were used for the $C^{18}O$ $J = 2 \rightarrow 1$ map, and these contours begin at 1.2 K km s^{-1} and increment by 0.2 K km s^{-1}. Contours for the $C^{17}O$ $J = 2 \rightarrow 1$ map start at 0.4 K km s^{-1} and increment by 0.1 K km s^{-1}. Locations of L1527A and L1527B are indicated by the star and triangle, respectively. Beam sizes of the observations are shown in the lower left of each panel.

FULLER, LADD, & HODAPP (see 463, L98)

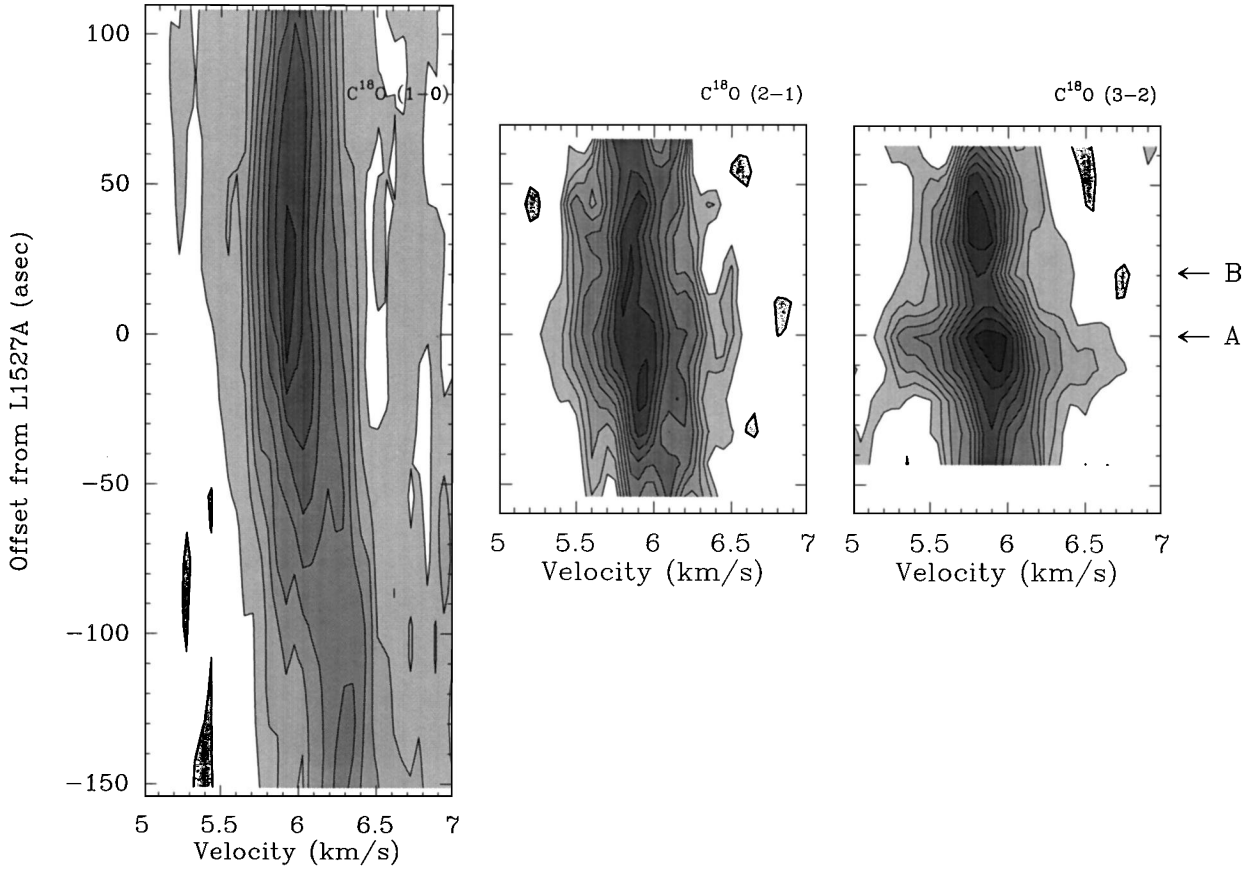

FIG. 4.—Position-velocity diagrams for the $J = 1 \rightarrow 0$, $J = 2 \rightarrow 1$, and $J = 3 \rightarrow 2$ transitions of $C^{18}O$ along the line joining L1527A and L1527B. The spatial resolution of the $J = 1 \rightarrow 0$ data is 60″, and the velocity resolution is 0.05 km s^{-1}. Contours start at 0.25 K and increment by 0.25 K. The spatial resolution of the $J = 2 \rightarrow 1$ data is 26″, and the velocity resolution is 0.1 km s^{-1}. Contours start at 0.75 K and increment by 0.25 K. The spatial resolution of the $J = 3 \rightarrow 2$ data is 26″, and the velocity resolution is 0.04 km s^{-1}. Contours start at 0.25 K and increment by 0.125 K. The position of L1527A and L1527B are labeled at right.

lines shows the same trend in velocity. Moving from the southeast toward L1527B, the velocity of the material decreases. Close to the position of L1527B, the velocity reaches a near minimum and remains nearly constant or increases slightly again to the northwest. A large velocity gradient was also found by Goodman et al. (1993) in NH_3 toward this core, though the position angle of the NH_3 gradient differs from that of the $C^{18}O$ $J = 1 \rightarrow 0$ gradient by ~50°.

The position-velocity diagrams (Fig. 4) of the $C^{18}O$ $J = 2 \rightarrow 1$ and $J = 3 \rightarrow 2$ delineate the velocity structure in the immediate environs of L1527A and L1527B. In the top contours of the $J = 2 \rightarrow 1$ image, and more clearly in the $J = 3 \rightarrow 2$ image, there appear to be two distinct velocity components: one is centered at a velocity of 5.8 km s^{-1} and is spatially associated with L1527B, and the other is centered at a velocity of 5.9 km s^{-1} and is better associated with L1527A. The velocity shift between the two clumps corresponds to a velocity gradient of ~3.5 km s^{-1} pc^{-1}, or a gradient of 7 km s^{-1} pc^{-1} for the 20″ separation of continuum components.

The line width of the $C^{17}O$ emission implies a virial mass of between 0.5 and 1 $M_\odot$, where the lower value corresponds to a sphere with an r^{-2} density profile and the higher value to a constant-density sphere. These values are in reasonable agreement with the ~0.5 $M_\odot$ of material detected in the $C^{17}O$, which indicates that the gas is within a factor of 2 of virial equilibrium.

4. DISCUSSION

The bulk of the luminosity of IRAS 04368+2557 is radiated at far-infrared wavelengths (Ladd et al. 1991a), where the low resolution of the *IRAS* beam does not resolve the L1527A/B system. If the two components have similarly shaped spectral energy distributions, the total luminosity of IRAS 04368+2557 can be divided between the A and B components in the ratio of their integrated 800 μm fluxes. For a total luminosity of 2 $L_\odot$ (Ladd et al. 1991a), the fluxes in Table 2 imply luminosities of 1.4 $L_\odot$ for L1527A and 0.7 $L_\odot$ for L1527B. A more accurate determination of the luminosity of each component of the system awaits further submillimeter and far-infrared observations that resolve this system.

Based on L1527B's 800 μm flux and implied luminosity, L1527B is most likely a self-luminous source. The small size and relatively large luminosity of L1527B compared to L1527A suggest that L1527B is not a clump of material directly heated by the radiation from L1527A. Its large luminosity also makes it unlikely that L1527B is a clump heated by the outflow from L1527A, since a significant fraction of the outflow luminosity would have to be deposited in this one clump that occupies only a small fraction of the volume of the outflow lobes (MacLeod et al. 1994). Further evidence that L1527B is a self-luminous source comes from the extended and elongated 160 and 100 μm far-infrared emission detected by Butner et al. (1994). The presence of a second source, with flux that is a reasonable fraction of that of the primary source in the 20″–30″ FWHM beam of the observations, could account for both the extended, elongated emission observed and the apparently shallow density profile inferred from the observations.

The separation of the L1527A/B system, ~2800 AU, is about twice the typical cutoff separation used to identify binary systems among T Tauri stars (Leinert et al. 1993; Simon et al. 1995). The probability that the second source is a chance line-of-sight projection of an unassociated source can be estimated from the density of *IRAS* sources in the region.

The dark cloud within which L1527A and L1527B reside, Heiles' Cloud 2, subtends about 1 square degree on the sky. Nine *IRAS* sources have been detected toward this cloud (Chen et al. 1995). Since L1527B is bright enough to have been detected by *IRAS* if it were located in a spatially unconfused field, we can estimate the probability of a chance alignment based on the surface density of known *IRAS* sources, 9/3600 or 2.5×10^{-3} arcmin^{-2}. If the sources are randomly distributed with a Poisson distribution, the probability that an unassociated *IRAS* source would be located within 20″ of L1527A is 9×10^{-4}. However, Gomez et al. (1993) have shown that the young stars in Taurus have a median separation 2–3 times smaller than for a random distribution. Including a factor of 3 in the median separation to increase the mean surface density by a factor of 9 increases the probability of a chance alignment to 8×10^{-3}. Although this probability estimate indicates that the presence of two sources as a result of a chance alignment cannot be ruled at the 3 standard deviation level, the properties of the system suggest that the two components are physically associated.

IRAS sources with steep spectral slopes are usually associated with regions of dense gas (Myers et al. 1987; Ladd, Myers, Goodman 1994), but the L1527 sources are located within a single well-defined dense core at the 0.1 pc size scale, with no evidence for a second 0.1 pc size core. Together with the relatively smooth velocity gradients in the $C^{18}O$ transitions tracing the molecular material associated with the A and B sources, and the small size of the gradient compared to the line width, this suggests that the two sources have formed from the same dense core, as against a chance line-of-sight alignment of two unassociated sources.

The age of IRAS 04368+2557 has been estimated to be $\sim 5 \times 10^3$ yr (Kenyon et al. 1993a), although age estimates based on the SED may need revision, since the presence of a secondary source means that the flux measured with the large beam of *IRAS* should not be assigned to a single young source. Nevertheless, given the large amount of circumstellar material associated with the L1527A source, and the absence of a near-infrared or optical counterpart (Tamura et al. 1991; Kenyon et al. 1993b), the source is probably very young. The 7 km s^{-1} pc^{-1} velocity gradient between the two $C^{18}O$ $J = 3 \rightarrow 2$ clumps associated with the continuum sources implies an orbital period of greater than 1.4×10^5 yr, more than an order of magnitude larger than the estimated age of the system, and comparable to the estimated lifetime of class I sources.

4.1. *Binary Formation*

Various models have been proposed for the formation of binary star systems. One class of models propose that binary systems are formed *after* the collapse of the dense gas into a star/disk system. Such models include binary formation through the fragmentation of massive circumstellar disks around the primary stars (Adams et al. 1989; Shu et al. 1990) and disk-aided capture of near companions (e.g., Clarke & Pringle 1991). Since the circumstellar disks have typical radii of ~100 AU, mechanisms for binary formation that invoke circumstellar disks tend to produce binary star systems with separations of ~100 AU or less. The relatively large separation of the two components of IRAS 04368+2557, ~2800 AU,

clearly rules out models for the formation of the secondary source through the fragmentation of a massive circumstellar disk around the primary source. The youth of the stars in the L1527 system and the long orbitial period, comparable to the estimated lifetime of class I sources, also rule out models for the formation of this system in which the stars form in isolation and the binary system forms only later through capture.

Other models for binary formation propose that binary systems form from the fragmentation of a core *during* collapse (e.g., Boss 1992 and references therein; Bonnell et al. 1991, 1992). Rotation plays an important role in these models, either as an important component in driving the fragmentation (Boss 1986) or to provide sufficient angular momentum to prevent fragments from coalescing (Bonnell et al. 1992). Since in the latter models the rotation around an axis perpendicular to the elongation of the original core only provides a centrifugal barrier, cores with smaller rotation gradients can form binary or multiple star systems. The models by Boss (1986) have initial conditions that are smaller and denser than the gas in the L1527. As a result, they form binaries with much smaller separations than the ~2800 AU separation of L1527A/B. On the other hand, Bonnell et al. (1991, 1992) predict that the fragments resulting from the collapse of an elongated cloud could be separated by up to ~10,000 AU.

The extreme youth of the L1527 protobinary system poses additional challenges for even these models of binary formation. In most models, there is no continuing infall of material from the larger scale core onto the forming binary system. However, the L1527A/B system is clearly associated with a large reservoir of surrounding material (Fig. 2) that, unless it is somehow supported or dispersed, will presumably collapse and accrete into the central region forming the young stars. Additionally, because of their youth, both A and B are likely to have outflows, which can significantly affect both the geometry and the dynamics of the circumbinary environment.

5. CONCLUSIONS

Continuum observations of the source IRAS 04368+2557 at 800 μm reveal that this source is a binary system. IRAS 04368+2557 therefore joins the small list of deeply embedded protobinary systems in nearby clouds, which includes NGC 1333 IRAS 4A/4B (Sandell et al. 1991) and IRAS 16293 (Wootten 1989; Mundy et al. 1992). If future observations show that multiplicity is common among the embedded low-luminosity sources, then the interpretation of spectral energy distributions, the spatial distribution of emission, velocity structure, and evidence for infall will need to be revised. Circumstantial evidence for a number of other embedded multiple systems comes from observations of multiple outflows that are suggestive of the presence of multiple sources (Hodapp & Ladd 1995).

The companion source, L1527B, has a luminosity one-half to one-third that of the primary source, if it has a similar spectral energy distribution to L1527A. The primary and secondary source are separated by ~2800 AU and are embedded in a single ~0.1 pc size core, traced by the $C^{17}O$ and $C^{18}O$ $J = 1 \rightarrow 0$ emission (Fig. 2) and NH_3 (Benson & Myers 1989). Three transitions of $C^{18}O$ all show velocity gradients along the line joining the two sources, demonstrating that the sources are physically associated, and placing a limit on the orbital energy in the system. Based on these observations, it appears likely that, at least in some cases, core fragmentation and binary formation occur at very early times in the formation of stellar systems, at a time when the young stars have still to accrete much of their final mass.

G. A. F. acknowledges the support of an NRAO Jansky Fellowship. G. A. F. thanks the Laboratory for Millimeter Wave Astronomy at the University of Maryland for their hospitality while he was writing parts of this Letter.

REFERENCES

Adams, F. C., Ruden, S. P., & Shu, F. H. 1989, ApJ, 347, 959
Benson, P. J., & Myers, P. C. 1989, ApJS, 71, 89
Bonnell, I., Arcoragi, J.-P., Martel, H., & Bastien, P. 1992, ApJ, 400, 579
Bonnell, I., Martel, H., Bastien, P., Arcoragi, J.-P., & Benz, W. 1991, ApJ, 337, 553
Boss, A. P. 1986, ApJS, 62, 519
Boss, A. P. 1992, in IAU Colloq. 135, Complementary Approaches to Double and Multiple Star Research, ed. H. A. McAlister & W. I. Hartkopf (San Francisco: ASP), 195
Butner, H. M., Moriarty-Schieven, G., Ressler, M. E., & Werner, M. W. 1994, Ap&SS, 224, 77
Chen, H., Myers, P. C., Ladd, E. F., & Wood, D. O. S. 1995, ApJ, 445, 377
Clarke, C. J., & Pringle, J. E. 1991, MNRAS, 249, 588
Ghez, A. M., Neugebauer, G., & Matthews, K. 1993, AJ, 106, 2005
Gomez, M., Hartmann, L., Kenyon, S. J., & Hewett, R. 1993, AJ, 105, 1927
Goodman, A. A., Benson, P. J., Fuller, G. A., & Myers, P. C. 1993, ApJ, 406, 528
Hodapp, K.-W., & Ladd, E. F. 1995, ApJ, 453, 715
Kenyon, S. J., Calvet, N., & Hartmann, L. 1993a, ApJ, 414, 676
Kenyon, S. J., Whitney, B. A., Gomez, M., & Hartmann, L. 1993b, ApJ, 414, 773
Ladd, E. F., Adams, F. C., Casey, S., Davidson, J. A., Fuller, G. A., Harper, D. A., Myers, P. C., & Padman, R. 1991a, ApJ, 366, 203
———. 1991b, ApJ, 382, 555
Ladd, E. F., Fuller, G. A., Padman, R., Myers, P. C., & Adams, F. C. 1995, ApJ, 439, 771
Ladd, E. F., Myers, P. C., & Goodman, A. A. 1994, ApJ, 433, 117
Leinert, Ch., Zinnecker, H., Weitzel, N., Christou, J., Ridgway, S. T., Jameson, R., Haas, M., & Lenzen, R. 1993, A&A, 278, 129
MacLeod, J., Lorne, A., Harris, A., Tacconi, L., & Schuster, K. 1994, JCMT Newsletter, September/October, 46
Mathieu, R. D., Walter, F. M., & Myers, P. C. 1988, AJ, 98, 987
Mundy, L. G., Wootten, A., Wilking, B. A., Blake, G. A., & Sargent, A. I. 1992, ApJ, 385, 306
Myers, P. C., Fuller, G. A., Mathieu, R. D., Benson, P. J., Beichman, C. A., Schild, R. E., & Emerson, J. P. 1987, ApJ, 319, 340
Myers, P. C., & Ladd, E. F. 1993, ApJ, 413, L47
Parker, N. D., Padman, R., & Scott, P. F. 1991, MNRAS, 252, 442
Pollack, J. B., Hollenbach, D., Beckwith, S., Simonelli, D. P., Roush, T., & Fong, W. 1994, ApJ, 421, 615
Reipurth, B., & Zinnecker, H. 1993, A&A, 278, 81
Sandell, G. 1994, MNRAS, 271, 75
Sandell, G., Aspin, C., Duncan, W. D., Russell, A. P., & Robson, E. I. 1991, ApJ, 376, 17
Shu, F. H., Tremaine, S., Adams, F. C., & Ruden, S. P. 1990, ApJ, 370, L31
Simon, M., Chen, W. P., Howell, R. R., Benson, J. A., & Slowik, D. 1992, ApJ, 384, 212
Simon, M., et al. 1995, ApJ, 443, 625
Tamura, M., Gatley, I., Waller, W., & Werner, M. W. 1991, ApJ, 347, L25
Terebey, S., Chandler, C. J., & André, P. 1993, ApJ, 414, 759
Wilner, D. 1996, in preparation
Wootten, A. 1989, ApJ, 337, 858